The Electrochemical Society
Advancing solid state & electrochemical science & technology

Reverse Breakdown in Large Area, Field-Plated, Vertical β-Ga$_2$O$_3$ Rectifiers

View the article online for updates and enhancements.

PR∑ME
PACIFIC RIM MEETING
ON ELECTROCHEMICAL
AND SOLID STATE SCIENCE
2020

Abstract Submission
DEADLINE EXTENDED:
May 29, 2020

Honolulu, HI | October 4-9, 2020

Reverse Breakdown in Large Area, Field-Plated, Vertical β-Ga₂O₃ Rectifiers

Jiancheng Yang,[1] Chaker Fares,[1,*] Randy Elhassani,[1] Minghan Xian,[1] Fan Ren,[1,]
S. J. Pearton,[2,**,z] Marko Tadjer,[3] and Akito Kuramata[4]**

[1]*Department of Chemical Engineering, University of Florida, Gainesville, Florida 32611, USA*
[2]*Department of Materials Science and Engineering, University of Florida, Gainesville, Florida 32611, USA*
[3]*Naval Research Laboratory, Washington, DC 20375, USA*
[4]*Tamura Corporation and Novel Crystal Technology, Inc., Sayama, Saitama 350-1328, Japan*

There is interest in developing large area Ga₂O₃ rectifiers for applications in hybrid power converters. Vertical geometry, Schottky rectifiers with area 1.2×1.2 mm² fabricated on thick (8μm), undoped (n = 4.4×10^{15} cm⁻³) β-Ga₂O₃ epitaxial layers oN conducting bulk substrates exhibit both high forward current (1A in pulsed mode) and reverse breakdown voltage (V_B = 760V). This breakdown voltage was ∼200V higher than rectifiers without the presence of a bilayer SiO₂/ SiNₓ field plate. This edge termination is critical for obtaining high breakdown voltage by reducing electric field crowding around the metal contact periphery. Optimization of the field plate design is still needed, since devices are observed experimentally to breakdown at the contact periphery. When purposely driven to failure at high reverse bias, pits are observed in the high field regions at the edge of the contact. The specific on-resistance (R_{on}) for these large area rectifiers was 22 mΩ.cm⁻², with a figure-of-merit V_B^2/Ron of 26 MW.cm⁻². The potential of Ga₂O₃ for power electronics is clear when it is realized that these values are still an order of magnitude lower than theoretical values. The diode on-off ratio was in the range 2.7×10^7–2.2×10^9 when switching from +1.5V forward bias to 1–100V reverse bias.

Wide-bandgap (WBG) devices are promising candidates for next-generation power electronics converters with higher efficiency and higher power conversion densities.[1–6] These inverters have applications in a range of power conditioning and control systems, including pulsed power for avionics and electric ships, solid-state drivers for heavy electric motors and in advanced power management and control electronics.[1–10] In addition, high-power (∼50kW) is required for fast wireless charging systems in transportation applications.[11] Highly efficient energy conversion for these systems is critical and this depends mainly on the ability of power switching transistors to provide low resistance in the on-state and highly resistive off-state conditions. To date, the focus has been on SiC and GaN to provide performance beyond Si.[1–5] High cost, challenging fabrication of practical devices, demonstrated reliability, and system integration remain important barriers to the widespread adoption of WBG devices.

A possible solution is hybrid switches, a combination of Si MOSFETs and wide bandgap devices. For example, hybrid modules containing Si MOSFETs and SiC rectifiers are commercially available.[12] One component of a switching module is a diode, most commonly Schottky rectifiers. These have fast switching speed, low forward voltage drop and high temperature operability.[8–10] Their advantage over p-n diodes is shorter switching times due to absence of minority carriers, but a disadvantage is higher on-state resistance (R_{ON}). Employing material with a wider bandgap than Si improves rectifier performance, with lower on-state resistance at a given reverse voltage.[1–5] Recently, Ga₂O₃ vertical geometry rectifiers have shown promising performance in terms of high reverse breakdown voltage (V_B> 1kV) and low R_{ON}, leading to good power figure-of-merits (V_B^2/R_{ON}).[11,13–46] Notable are reverse breakdown voltages (V_B) of 2300V for a 150 μm diameter device (area = 1.77×10^{-4} cm⁻²)[47] and 2440 V breakdown in trench structures.[48] Another potential advantage of Ga₂O₃ are the lower substrate costs compared to SiC.[32–42] Reese et al.[40] used techno-economic modeling of Ga₂O₃ wafer cost based on future large-size and high-volume manufacturing scenarios and estimated there could be a >3x cost advantage compared to SiC wafers. This could lead to a significant cost reduction for wide-bandgap power electronics.[49–52]

In current Ga₂O₃ rectifiers, breakdown resulting from impact ionization preferentially occurs at the contact periphery unless the electric field is reduced by edge termination.[5,27] Baliga's figure of merit (FOM) ($\varepsilon_r\mu Ebr^3$) where ε_r is relative dielectric constant and μ is mobility[7,8,42–46] is 4x larger for β-Ga₂O₃ than SiC and GaN.[5–10] The theoretical breakdown field for Ga₂O₃ is between 5–9 MV/cm, with peak experimental values of 5.3 MV.cm⁻¹.[31] Lateral structures have shown breakdown voltages of over 3kV.[29] The switching characteristics of Ga₂O₃ vertical Schottky rectifier show recovery times of 20–30 ns,[45,46,48,49,53] faster than Si or SiC diodes.

Vertical geometry, large area planar devices can produce large total forward currents, while maintaining adequate reverse breakdown.[45–58] This is a stringent test of material quality, since large diodes increase the probability of incorporating defects into the active region, degrading reverse breakdown voltage.[37,39,43,45] Lateral devices can achieve high breakdown voltage using large contact separations, but cannot simultaneously achieve high forward current due to the low total conduction thickness. They also have high on-state resistance.[45,48]

In this paper, we show vertical geometry Schottky rectifiers with a minimum of process steps can achieve forward currents of 1 A at 2.3 V and reverse breakdown voltages of 760 V for large (0.14 cm²) devices, emphasizing the potential of Ga₂O₃ for majority carrier switching devices.

Experimental

Epitaxial layers (∼8 μm final thickness) of lightly Si-doped n-type (4.36×10^{15} cm⁻³) Ga₂O₃ were grown by Halide Vapor Phase Epitaxy (HVPE) on n⁺ (3.6×10^{18} cm⁻³), β-phase Sn-doped Ga₂O₃ wafers (∼650 μm thick) with (001) surface orientation grown by the edge-defined film-fed method.[17,18] The design of the edge termination was guided by device simulations using the MEDICI code of breakdown voltage with various thicknesses, overlap and type of dielectric used in the field plate. The main findings were that the use of an optimized field plate edge termination can increase the reverse breakdown voltage of vertical Ga₂O₃ rectifiers by up to a factor of two compared
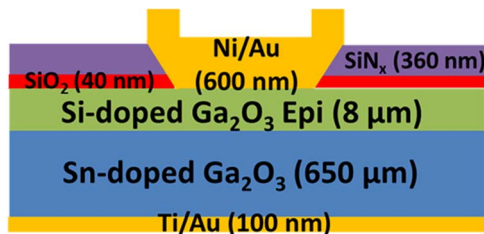
Figure 1. Schematic of vertical β-Ga$_2$O$_3$ Schottky rectifier utilizing a bilayer SiO$_2$/SiN$_x$ field plate.

to unterminated devices. Moreover, the dielectric material, thickness (and ramp angle if using a bevel edge termination) all influence the resulting V$_B$ of the rectifier by determining where the maximum field strength occurs in the device structure. The key aspect in designing the field plate edge termination is to shift the region of the high field region away from the periphery of the rectifying contact. Ar implantation,[58] beveling[42] or use of trenches[48] have also been shown to reduce field crowding in Ga$_2$O$_3$ rectifiers. However, these add complexity to the fabrication relative to simple field plates and in the case of trenches, reduce the current capability.

The rectifiers employed back ohmic contacts (20 nm Ti/80 nm Au) deposited by E-beam evaporation. These contacts were annealed at 550°C for 30 s in N$_2$. The epi surface was treated with ozone for 10 min to remove adventitious carbon contamination, followed by deposition of 40 nm of SiO$_2$ and 360 nm of SiN$_x$ by plasma enhanced chemical vapor deposition at 300°C using silane and ammonia precursors. This field plate reduces the maximum electric field around the rectifying contact periphery.[1–4,27,55] The SiO$_2$/SiN$_x$ contact windows were lithographically patterned and opened with 1:10 buffered oxide etch (BOE) at 25°C. The front Schottky contacts were overlapped 10 μm on the SiO$_2$/SiN$_x$ window openings by lift-off of E-beam deposited Ni/Au (120 nm/480 nm). This geometry was guided by the simulations discussed above. The size of these contacts was fixed at 0.12 cm × 0.12 cm. In a few cases, we made smaller diodes and these were found to have higher reverse breakdown (in the range 800–1100V), but their total forward currents were also smaller and in this paper we focused on achieving high numbers for both. Figure 1 shows a schematic of the rectifier. The current-voltage (I-V) and capacitance-voltage (C-V) characteristics were measured in air at 25–150°C on an Agilent 4145B parameter analyzer and 4284A Precision LCR Meter. For reverse voltages >100 V and forward currents >100 mA, a Tektronix 370A curve tracer was used due to the limitation of the Agilent analyzer.

Results and Discussion

Figure 2 shows the C^{-2}–V characteristics used to obtain the drift layer n-type donor concentrations (N$_D$). The value of 4.36 ×
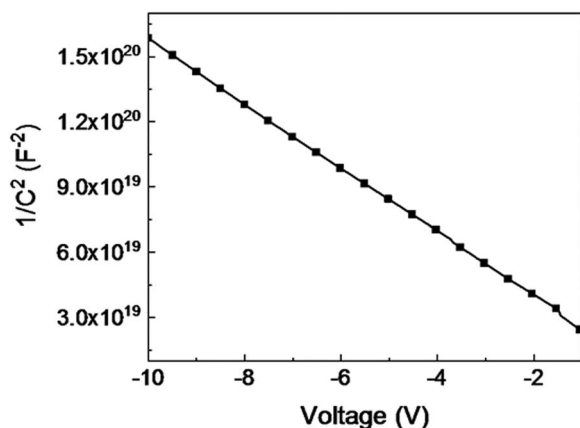
**Figure 2.** Plot of C^{-2}-V to determine carrier density in drift region.
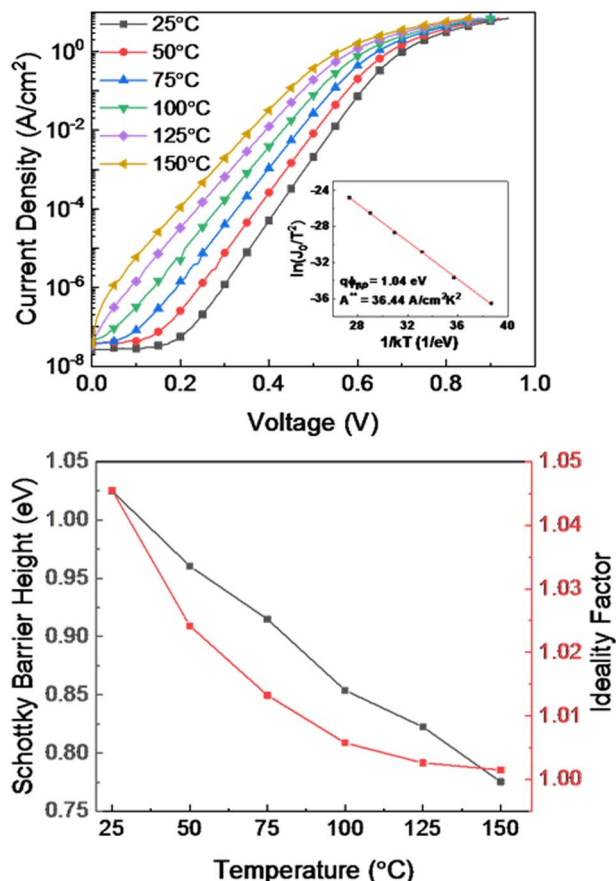
Figure 3. (top) Temperature dependence of forward current. The inset shows the Richardson plot derived from the forward J-V-T data.(bottom) temperature dependence of φ$_b$ and ideality factor.

10^{15} cm^{-3} shows epitaxial layers of β-Ga$_2$O$_3$ can be controllably doped at low enough levels to sustain a large reverse bias while still having good forward characteristics.

Figure 3 (top) shows the temperature dependence of forward current (I-V) characteristics. The zero voltage barrier height eΦ$_{b0}$ (e is electronic charge and Φ$_b$ is barrier height) was determined from the forward current density (J)-voltage-temperature (J-V-T) characteristics by linear fitting of the Richardson's plot (inset of Figure 3). This was 1.04 eV, with a Richardson's constant of 36.44 A.cm^{-2}.K^{-2}, comparable to the values reported[23,24] for Pt of 1.15 eV and 55 A.cm^{-2} K^{-2}. Figure 3 (bottom) shows the temperature dependence of Φ$_b$ and ideality factor *n* for 25–125°C. The barrier height decreases with temperature, as expected in pure thermionic emission.[55–57] For these lightly doped layers, *n* should be close to unity, with a small increase due to the image force effect.[27] The ideality factor improves with temperature, reaching 1.00 at 150°C, useful for elevated temperature operation.

The single sweep forward current density (J-V) characteristic is shown in Figure 4 (top). The forward current reached 1 A at 2.3 V. In this mode, the collector supply sweeps from 0 V to its preselected value. During the sweep, 1% duty cycle of a 280 μsec pulse width was employed. The on-state resistance was 22.3 mΩ.cm^2.

As an independent check on this data, the model of Cheung and Cheung[56] was applied to extract Φ$_b$, *n* and series resistance R. Since V = RAJ + nΦ$_B$ + (nkT/e)ln(J /A**T^2), then d (V)/d(lnJ) = RAJ + nkT/e, where A is the rectifier area, A** is Richardson's constant, k is Boltzmann's constant, T is measurement temperature. Thus, a plot of d (V)/d(ln J) vs J will give RA as the slope and nkT/e as the y-axis intercept.[56] This data is shown in Figure 4 (bottom).The barrier height is extracted by defining the function H (J) = V - (nkT/e) In(J /A**T^2) which is also equal to RAJ+nΦ$_b$. Using the n value determined from
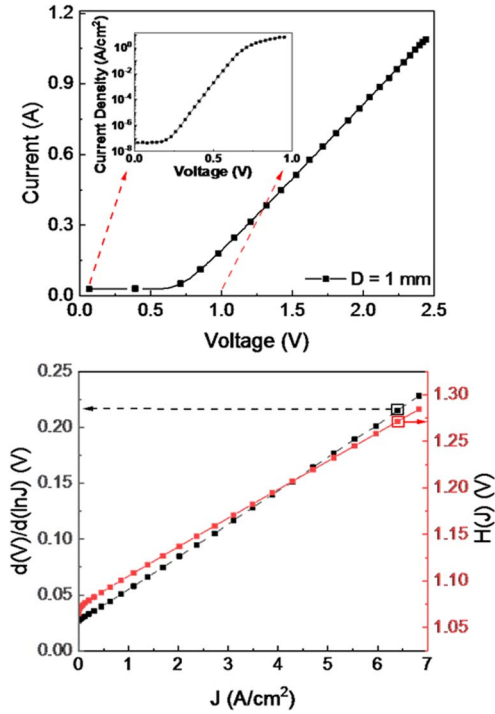
Figure 4. (top) Forward J-V characteristic of rectifier. The inset shows the data on a log scale. (bottom) plot of $d(V)/d(\ln J)$ vs J to extract barrier height.

the plot of $d(V)/d(\ln J)$ vs J, a plot of H(J) vs J will also give a straight line with y-axis intercept equal to n Φ_b. We obtained R_{ON} values of 29.2 m $\Omega.cm^2$ from the $d(V)/d(\ln J)$ data and 32.4m$\Omega.cm^2$ from the H(J) analysis, in agreement with the thermionic emission analysis.

Figure 5 (top) shows the reverse breakdown voltage is 760 V, so the figure of merit (V_B^2/R_{ON}) is 26 MW.cm^{-2}. Rectifiers with much smaller areas ($\sim 10^{-5}$ cm^2) exhibit higher values of
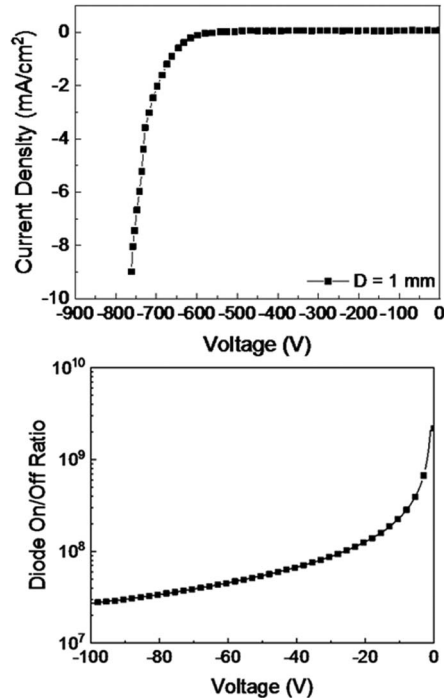

Figure 5. (top) Reverse current density as a function of voltage. (bottom) Rectifier on-off ratio as a function of reverse bias. The on-current was 1 A at 2.3V and the on-off ratio range measured was 3.3×10^9–5.7×10^6.
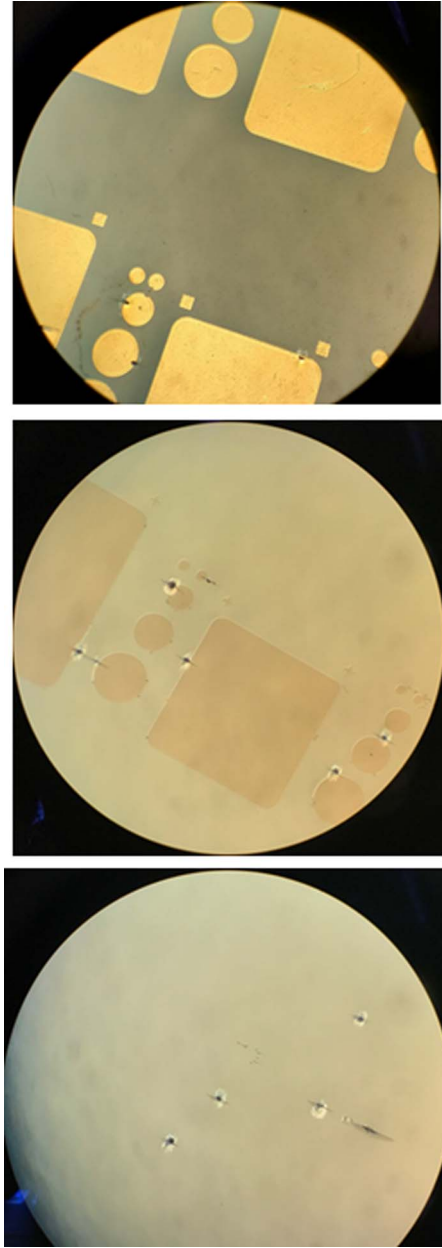
Figure 6. Optical microscope images of rectifiers after reverse breakdown failure. The top image shows the sample with contacts in place, the middle image after Au/Ni etching to remove the contact and the bottom image shows the same area after BOE soaking.

102–154 MW.cm^{-2},[15,16,24–30] but those devices had lower total forward currents. The 760V breakdown voltage is applicable to efficient power switching in systems for photovoltaic, wind energy and motor drives.[11,12,40] Figure 5 (bottom) shows the on/off current ratio was in the range 2.7×10^7–2.2×10^9 when switching from +1.5V forward bias to 1–100V reverse bias. This is better than the previous report,[53] due to continued improvement in epitaxial doping control. The reverse recovery time when switching from +2V to −10V, was 33.5 ns, comparable to devices with much smaller rectifier dimensions.[14,26,49] More detailed measurements of the diode recovery time to the current level of 25% of the reverse recovery current using a clamped inductive load test circuit showed that for switching from 1A forward current to −300V reverse bias, the recovery time was 64 ns with I_{rr} of 0.82 A, and the dI/dt was 24.7 A/μs.[58] These values are comparable to previously reported Ga$_2$O$_3$ trench MOS Schottky diodes, Si-fast recovery

Breakdown Voltage Caused Defect (Top View)
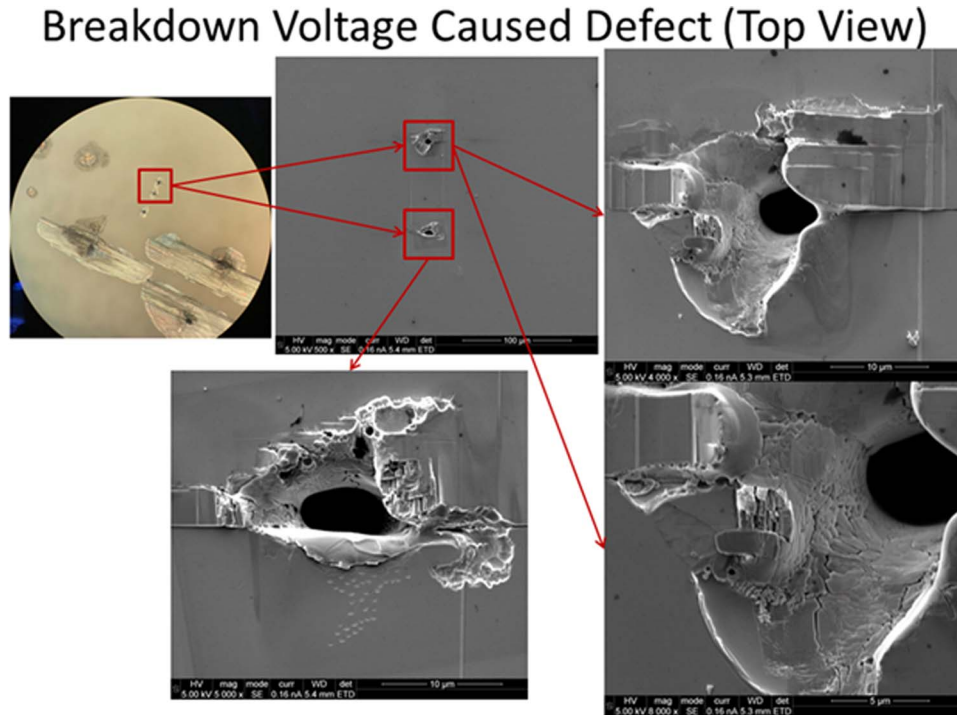
Figure 7. Optial microscope image and close-up SEM images of the pits formed as a result of failure under reverse bias breakdown.

diodes (FRDs, Rohm RF1005TF6S) and SiC Schottky barrier diodes from Cree (part number C3D0260A) for turn-off from $I_F = 1$ A.[49]

It is also worth noting the rectifiers when pushed to failure under reverse bias conditions, showed formation of pits along the periphery of the Schottky contact. An example is shown in Figure 7, which shows optical microscope images of the pits formed at the contact edge. The pits are clearer after etch removal of the Au/Ni contact. Figure 8 shows scanning electron microscopy images of these pits, which result from avalanche failure of the Ga_2O_3 under the high field generated at the edge of the rectifying contact. These results indicate that further optimization of the edge termination material and geometry is needed to reduce field crowding.

To put our results in context with the previous literature on Ga_2O_3 and also the performance of SiC and GaN rectifiers, our β-Ga_2O_3 rectifiers are benchmarked in the plot of specific R_{ON} versus V_b in Figure 8 (top). This also shows the relation between breakdown voltage, electric field and doping in vertical geometry rectifier consisting of a lightly doped drift region on a more heavily doped layer on a conducting substrate of these respective materials. Experimental points for Ga_2O_3 from different groups[19,21,22,25–28,34,35,46–48,57] are also shown-these are not yet at the values achieved by the smaller bandgap SiC and GaN, where the theoretical limits are now being approached. Continued development of low defect substrates, optimized epi growth and surface treatments and improved device design and processing methods for Ga_2O_3 are still required to push the experimental results closer to their theoretical values. Table I also shows a detailed compilation of vertical rectifier results from the literature.

Figure 8 (bottom) is a plot of theoretical breakdown voltage of Ga_2O_3 vertical punchthrough diodes as a function of doping concentration and drift region thickness. This assumes the breakdown voltage is given by $V_B = E_C W - [e N_B W^2 / 2 \varepsilon \varepsilon_r]$, where E_C is the critical field for breakdown, W is the depletion depth, N_B the doping concentration

Table I. Summary of vertical geometry Ga_2O_3 rectifiers reported in literature.

Reference	Epi Thickness(μm)	Drift Layer Doping (cm^{-3})	Edge Termination	V_B (V)	R_{ON} (Ω.cm^2)
Konishi et al.[27]	10	1.8×10^{16}	Yes-field plate	1076	5.1×10^{-3}
Yang et al.[25]	10	4.02×10^{15}	No	1600	25×10^{-3}
Yang et al.[26]	10	2×10^{16}	No	1016	6.7×10^{-3}
Sasaki et al.[21]	Unintentionally doped substrate	3×10^{16}	No	150	4.3×10^{-3}
Li et al.[28]	10	2×10^{16}	Trench	1350	15×10^{-3}
Li et al.[48]	10	2×10^{16}	Trench	2440	25×10^{-3}
Oh et al.[38]	2	Undoped, $< 3 \times 10^{16}$	No	210	2582
He et al.[22]	Unintentionally doped substrate	2×10^{14}	No	>40	12.5×10^{-3}
Tadjer et al.[34]	~10	8×10^{12}	No	2380	n/a
Fu et al.[35]	Sn-doped EFG substrates	4×10^{18}	No	low	0.77×10^{-3}
Joishi et al.[42]	2	2.5×10^{17}	Bevel	190	3.9×10^{-3}
Yang et al.[46]	10	1.33×10^{16}	Yes-field plate	650	1.58×10^{-2}
Yang et al.[47]	20	2.1×10^{15}	Yes-field plate	2300	0.25
Yang et al.[48]	7	2×10^{16}	No	466	$0.26–5.9 \times 10^{-4}$
Li[57]	15, exfoliated	Sn doped	No	97	2.1×10^{-3}
Gao et al.[19]	10, exfoliated	Sn doped	Ar implantation	550	1.7×10^{-3}
This work	8	4.4×10^{15}	Yes-field plate	760	22.2×10^{-3}
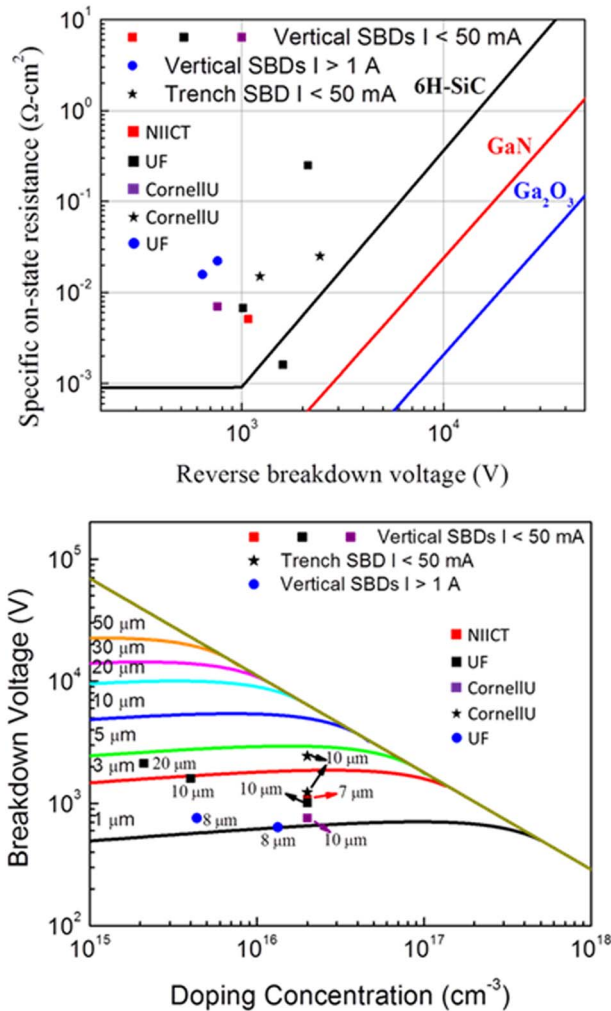
Figure 8. (top) The reverse breakdown voltage of punch-through junctions for Ga_2O_3 as a function of doping concentration and drift region thickness.(bottom) Specific R_{ON} versus V_B of state-of-the-art vertical β-Ga_2O_3 rectifiers.

and ε_r and ε the relative and absolute permittivity. Even 3 μm epi layers with doping concentration of 10^{16} cm^{-3} should have a theoretical breakdown voltage of $\sim$1800V. The actual experimental value of V_B is well below the theoretical predictions. Our case of 8 μm with doping 4.4×10^{15} cm^{-3} has a theoretical breakdown more than an order of magnitude larger than the experimental value.[43,44]

Conclusions

The initial thrust on Ga_2O_3 electronics is targeted toward high power converters for both DC/DC and DC/AC applications. Schottky barrier diodes on β-Ga_2O_3 have achieved a breakdown strength of $\sim$4 MV/cm. The question remains as to whether Ga_2O_3 will have commercial advantages over the more mature SiC and GaN technology for power switching and power amplifier applications. While the initial device performance looks promising, challenges remain, including growth maturity, thermal limits, cost, and device reliability. The results summarized here show the potential of β-Ga_2O_3 for fast-switching power devices, capable of simultaneously achieving both high on-state currents and breakdown voltages. The use of thick, lightly doped epitaxial drift regions enable realization of large dimension (0.014 cm^2) β-Ga_2O_3 Schottky rectifiers with large forward current (1A), V_{BR} values of 760 V and power density figures of merit of 26 MW.cm^{-2}. Since power converters require the power device to switch at high frequen-

cies for improved dynamic response capability and reduced passive component size and weight, the performance of these Ga_2O_3 rectifiers is consistent with these goals. It is likely that Ga_2O_3 will not displace materials such as SiC and GaN, but possibly supplement them at high voltages in hybrid systems.

ORCID

Chaker Fares https://orcid.org/0000-0001-9596-2381
Fan Ren https://orcid.org/0000-0001-9234-019X
S. J. Pearton https://orcid.org/0000-0001-6498-1256
Marko Tadjer https://orcid.org/0000-0002-2388-2937

References

1. Alex Q. Huang, *Proc. IEEE*, **105**, 2019 (2017).
2. X. She X, A. Q. Huang, O. Lucıa, and B. Ozpineci, *IEEE Trans. Ind. Electron.*, **64**, 8193 (2017).
3. H. Amano, Y. Baines, E. Beam, M. Borga, T. Bouchet, P. R. Chalker, M. Charles, K. J. Chen, N. Chowdhury, R. Chu, C. De Santi, M. M. De Souza, D. Decoutere, L. Di Cioccio, B. Eckardt, T. Egawa, P. Fay, J. J. Freedsman, L. Guido, O. Häberlen, G. Haynes, T. Heckel, D. Hemakumara, P. Houston, J. Hu, M. Hua, Q. Huang, A. Huang, S. Jiang, H. Kawai, D. Kinzer, M. Kuball, M. Kumar, K. D. Lee, X. Li, D. Marcon, M. März, R. McCarthy, G. Meneghesso, M. Meneghini, E. Morvan, A. Nakajima, E. Narayanan, S. Oliver, T. Palacios, D. Piedra, M. Plissonnier, R. Reddy, M. Sun, I. Thayne, A. Torres, U. N. Trivellin, M. Uren, M. Van Hove, D. Wallis, J. Wang, J. Xie, S. Yagi, S. Yang, C. Youtsey, R. Yu, E. Zanoni, S. Zeltner, and Y. Zhang, *J. Phys. D: Appl. Phys.*, **51**, 163001 (2018).
4. T. J. Flack, B. N. Pushpakaran, and S. B. Bayne, *J. Electron. Mater.*, **45**, 2673 (2016).
5. J. Y. Tsao, S. Chowdhury, M. A. Hollis, D. Jena, N. M. Johnson, K. A. Jones, R. J. Kaplar, S. Rajan, C. G. Van de Walle, E. Bellotti, C. L. Chua, R. Collazo, M. E. Coltrin, J. A. Cooper, K. R. Evans, S. Graham, T. A. Grotjohn, E. R. Heller, M. Higashiwaki, M. S. Islam, P. W. Juodawlkis, M. A. Khan, A. D. Koehler, J. H. Leach, U. K. Mishra, R. J. Nemanich, R. C. N. Pilawa-Podgurski, J. B. Shealy, Z. Sitar, M. J. Tadjer, A. F. Witulski, M. Wraback, and J. A. Simmons, *Adv. Electron. Mater.*, **4**, 1600501 (2018).
6. M. Higashiwaki, A. Kuramata, H. Murakami, and Y. Kumaga, *J. Phys. D: Appl. Phys.*, **50**, 333002 (2017).
7. Masataka Higashiwaki and Gregg H, Jessen, *Appl. Phys. Lett.*, **112**, 060401 (2018).
8. B. Bayraktaroglu, Assessment of Gallium Oxide Technology, Air Force Research Lab, Devices for Sensing Branch, Aerospace Components & Subsystems Division, Report AFRL-RY-WP-TR-2017-0167., 2017, http://www.dtic.mil/dtic/tr/fulltext/u2/1038137.pdf
9. Michael A. Mastro, Akito Kuramata, Jacob Calkins, Jihyun Kim, Fan Ren, and S. J. Pearton, *ECS J. Solid State Sci. Technol.*, **6**, P356 (2017).
10. S. J. Pearton, Jiancheng Yang, Patrick H. Cary, F. Ren, Jihyun Kim, Marko J. Tadjer, and Michael A. Mastro, *Appl. Phys. Rev.*, **5**, 011301 (2018).
11. S. J. Pearton, Fan Ren, Marko Tadjer, and Jihyun Kim, *J. Appl. Phys.*, **124**, 220901 (2018).
12. https://www.infineon.com/cms/en/product/power/wide-band-gap-semiconductors-sic-gan/silicon-carbide-sic/
13. Xue Hui Wen, He QiMing, Jian Guang Zhong, Long Shi Bing, Pang Tao, and Liu Ming, *Nanoscale Res. Lett*, **13**, 290 (2018).
14. Yangyang Gao, Ang Li, Qian Feng, Zhuangzhuang Hu, Zhaoqing Feng, Ke Zhang, and Xiaoli Lu, *Nanoscale Res. Lett.*, **14**, 8 (2019).
15. Chunfu Zhang, Hong Zhou, Wenxiang Mu, Zhitai Jia, Jincheng Zhang, Yue Hao, Zeng Liu, Pei-Gang Li, Yu-Song Zhi, Xiao-Long Wang, Xu-Long Chu, and Wei-Hua Tang, *Chinese Phys. B.*, **28**,017105 (2019).
16. Bo Fu, Zhitai Jia, Wenxiang Mu, Yanru Yin, Jian Zhang, and Xutang Tao, *J. Semicond.*, **40**, 011804 (2019).
17. Hong Zhou, Jincheng Zhang, Chunfu Zhang, Qian Feng, Shenglei Zhao, Peijun Ma, and Yue Hao, *J. Semicond.*, **40**, 011803 (2019).
18. Read more at: https://phys.org/news/2018-12-gallium-oxide-ultrawide-bandgap-semiconductor.html#jCp
19. S. Rafique, L. Han, A. T. Neal, S. Mou, M. J. Tadjer, R. H. French, and H. Zhao, *Appl. Phys. Lett.*, **109**, 132103 (2016).

20. M. J. Tadjer, N. A. Mahadik, V. D. Wheeler, E. R. Glaser, L. Ruppalt, A. D. Koehler, K. D. Hobart, C. R. Eddy, and F. J. Kub, *ECS J. Solid State Sci. Technol.*, **5**, P468 (2016).

21. K. Sasaki, M. Higashiwaki, A. Kuramata, T. Masui, and S. Yamakoshi, *IEEE Electron Device Lett.*, **34**, 493 (2013).

22. Q. He, W. Mu, H. Dong, S. Long, Z. Jia, H. Lv, Q. Liu, M. Tang, X. Tao, and M. Liu, *Appl. Phys. Lett.*, **110**, 093503 (2017).

23. T. Oishi, Y. Koga, K. Harada, and M. Kasu, *Appl. Phys. Express*, **8**, 031101 (2015).

24. M. Higashiwaki, K. Konishi, K. Sasaki, K. Goto, K. Nomura, Q. T. Thieu, R. Togashi, H. Murakami, Y. Kumagai, B. Monemar, A. Koukitu, A. Kuramata, and S. Yamakoshi, *Appl. Phys. Lett.* **108**, 133503 (2016).

25. J. Yang, S. Ahn, F. Ren, S. J. Pearton, S. Jang, J. Kim, and A. Kuramata, *Appl. Phys. Lett.*, **110**, 192101 (2017).

26. J. Yang, S. Ahn, F. Ren, S. J. Pearton, S. Jang, and A. Kuramata, *IEEE Electron Device Lett.*, **38**, 906 (2018).

27. Keita Konishi, Ken Goto, H. Murakami, Y. Kumagai, Akito Kuramata, Shigenobu Yamakoshi, and Masataka Higashiwaki, *Appl. Phys. Lett.*, **110**, 103506 (2017).

28. Wenshen Li, Zongyang Hu, Kazuki Nomoto, Zexuan Zhang, Jui-Yuan Hsu, Quang Tu Thieu, Kohei Sasaki, Akito Kuramata, Debdeep Jena, and Huili Grace Xing, *Appl. Phys. Lett.* **113**, 202101 (2018).

29. Zongyang Hu, Kazuki Nomoto, Wenshen Li, Zexuan Zhang, Nicholas Tanen, Quang Tu Thieu, Kohei Sasaki, Akito Kuramata, Tohru Nakamura, Debdeep Jena, and Huili Grace Xing, *Appl. Phys. Lett.* **113**, 122103 (2018).

30. H. Zhou Z.Hu and Q. Feng, *IEEE Electron Device Lett*, **39**, 1564 (2018).

31. Marko J. Tadjer, Andrew D. Koehler, Jaime A. Freitas Jr., James C. Gallagher, Matty C. Specht, Evan R. Glaser, Karl D. Hobart, Travis J. Anderson, Fritz J. Kub, Quang T. Thieu, Kohei Sasaki, Daiki Wakimoto, Ken Goto, Shinya Watanabe, and Akito Kuramata, *Appl. Phys. Lett.* **113**,192102 (2018).

32. A. J. Green, K. D. Chabak, E. R. Heller, R. C. Fitch, M. Baldini, A. Fiedler, K. Irmscher, G. Wagner, Z. Galazka, S. E. Tetlak, A. Crespo, K. Leedy, and G. H. Jessen, *IEEE Electron Device Lett.*, **37**, 902 (2016).

33. Janghyuk Kim, Michael A. Mastro, Marko J. Tadjer, and Jihyun Kim, *ACS Appl. Mater. Interf.*, **9**, 21322 (2017).

34. M. J. Tadjer, A. D. Koehler, N. A. Mahadik, E. Glaser, J. A. Freitas, B. Feigelson, V. D. Wheeler, K. D. Hobart, F. J. Kub, and A. Kuramata, Thick, Low-Doped Homoepitaxial Ga$_2$O$_3$ for Power Electronics Applications, 232nd ECS Meeting, October 1 - 5, 2017, National Harbor, Maryland.

35. Houqiang Fu, Hong Chen, Xuanqi Huang, Izak Baranowski, Jossue Montes, Tsung-Han Yang, and Yuji Zhao, *IEEE Trans Electron Dev*, **65**, 3507 (2018).

36. J. Bae, H. W. Kim, I. H. Kang, G. Yang, and J. Kim, *Appl. Phys. Lett.*, **112**, 122102 (2018).

37. T. Oishi, Y. Koga, K. Harada, and M. Kasu, *Appl. Phys. Express*, **8**, 31101(2015).

38. S. Oh, G. Yang, and J. Kim, *ECS J. Solid State Sci. Technol.*, **6**, Q3022 (2017).

39. M. Oda, R. Tokuda, H. Kambara, T. Tanikawa, S. Sasaki, and T. Hitora, *Appl. Phys. Express*, **9**, 021101 (2016).

40. Samantha B. Reese, Timothy Remo, Johney Green, and Andriy Zakutayev, *Gallium Oxide Power Electronics: Towards Silicon Cost and Silicon Carbide Performance*, Joule (in press, 2019).

41. M. J. Tadjer, V. D. Wheeler, D. I. Shahin, C. R. Eddy, and J. Fritz, *KubECS J. Solid State Sci. Technol.*, **6**, P165 (2017).

42. C. Joishi, S. Rafique, Z. Xia, L. Han, S. Krishnamoorthy, Y. Zhang, Y. Lodha, H. Zhao, and S. Rajan, *Appl. Phys. Exp.*, **11**, 031101 (2018).

43. M. Kasu, K. Hanada, T. Moribayashi, A. Hashiguchi, T. Oshima, T. Oishi, K. Koshi, K. Sasaki, A. Kuramata, and O. Ueda, *Jpn. J. Appl. Phys.*, **55**, 1202BB (2016).

44. T. Oshima, A. Hashiguchi, T. Moribayashi, K. Koshi, K. Sasaki, A. Kuramata, O. Ueda, T. Oish, and M. Kasu, *Jpn. J. Appl. Phys.*, **56**, 086501 (2017).

45. M. J. Tadjer, N. A. Mahadik, J. A. Freitas, E. R. Glaser, A. D. Koehler, L. E. Luna, B. Feigelson, K. D. Hobart, F. J. Kub, and A. Kuramata, *Proc. SPIE 10532, GaN Materials and Devices XIII*, **2018**, 1053212 (2018).

46. J. C. Yang, F. Ren, M. J. Tadjer, S. J. Pearton, and A. Kuramata, *AIP Advances*, **8**, 055026 (2018).

47. J. C. Yang, F. Ren, M. J. Tadjer, S. J. Pearton, and A. Kuramata, *ECS J Solid State Sci Technol*, **7**, Q92 (2018).

48. Wenshan Li, Z. Hu, K. Nomoto, R. Jinno, Z. Zhang, T. Q. Tu, K. Sasaki, A. Kuramata, D. Jena, and H. Grace Xing, 2.44 kV Ga$_2$O$_3$ vertical trench Schottky barrier diodes with very low reverse leakage current, *2018 IEEE International Electron Devices Meeting (IEDM)* pp. 8.5.1 (2018).

49. Akio Takatsuka, Kohei Sasaki, Daiki Wakimoto, Quang Tu Thieu, Yuki Koishikawa, Jun Arima, Jun Hirabayashi, Daisuke Inokuchi, Yoshiaki Fukumitsu, Akito Kuramata, and Shigenobu Yamakoshi, *2018 76th Device Research Conference (DRC)*, pp. 1, June 2018.

50. Q. He, W. Mu, B. Fu, Z. Jia, S. Long, Z. Yu, Z. Yao, W. Wang, H. Don, and Y. Qin, *IEEE Electron Device Lett*, **39**, 556 (2018).

51. K. Sasaki, D. Wakimoto, Q. T. Thieu, Y. Koishikawa, A. Kuramata, M. Higashiwaki, and S. Yamakoshi, *IEEE Electron Device Lett.* **38**, 783 (2017).

52. G. Jian G, Q. He, W. Mu, B. Fu, H. Dong, Y. Qin, Y. Zhang, H. Xue, S. Lon, and Z. Jia, *AIP Adv* **8**, 015316 (2018).

53. Zongyang Hu, Kazuki Nomoto, Wenshen Li, Nicholas Tanen, Kohei Sasaki, Akito Kuramata, Tohru Nakamura, Debdeep Jena, and Huili Grace Xing, *IEEE Electron Dev. Lett.* **39**, 869 (2018).

54. J. C. Yang, F. Ren, S. J. Pearton, and A. Kuramata, *IEEE Trans Electron Dev*, **265**, 2790 (2018).

55. B. J. Baliga, *IEEE Electron Dev. Lett.*, **10**, 455 (1989).

56. S. Ahn, F. Ren, L. Yuan, S. J. Pearton, and A. Kuramata, *ECS J. Solid State Sci. Technol.* **6**, P68 (2017).

57. S. K. Cheung and N. W. Cheung, *Appl. Phys. Lett.*, **49**, 85 (1986).

58. Ang Li, Qian Feng, Jincheng Zhang, Zhuang Hu, Zhaoqing Feng, Ke Zhang, Chunfu Zhang, Hong Zhou, and Yue Hao, *Superlatt. Microstr.* **119**, 212 (2018).

59. Jiancheng Yang, Fan Ren, YenTing Chen, Yu Te Liao, Chin Wei Chang, Jenshan Lin, Marko J. Tadjer, S. J. Pearton, and Akito Kuramata, *IEEE Journal of the Electron Devices Society*, **7**, 57 (2018).